

ON THE NUMERICAL SIGNATURE OF BLOW-UP IN HYDRODYNAMIC EQUATIONS

ERIK JANSSON^{*,†} AND KLAS MODIN^{*}

ABSTRACT. The phenomenon of finite time blow-up in hydrodynamic partial differential equations is central in analysis and mathematical physics. While numerical studies have guided theoretical breakthroughs, it is challenging to determine if the observed computational results are genuine or mere numerical artifacts. Here we identify numerical signatures of blow-up. Our study is based on the complexified Euler equations in two dimensions, where instant blow-up is expected. Via a geometrically consistent spatiotemporal discretization, we perform several numerical experiments and verify their computational stability. We then identify a signature of blow-up based on the growth rates of the supremum norm of the vorticity with increasing spatial resolution. The study aims to be a guide for cross-checking the validity of future numerical experiments of suspected blow-up in equations where the analysis is not yet resolved.

Keywords: Euler equations, blow-up, matrix hydrodynamics, Zeitlin’s model, Euler-Arnold equations, PDE numerics, vorticity

MSC2010: 35Q31, 35B44, 81S10, 65G50, 65M12

1. INTRODUCTION

Finite time blow-up in hydrodynamic equations is an active topic in the analysis of partial differential equations (PDEs). For the 3-D incompressible Euler equations, significant results were given by Elgindi [9] and by Chen and Hou [7]. These results were partially guided by numerical simulations of Luo and Hou [16], whose work thus exemplifies how careful numerical experiments can lead to theoretical breakthroughs. On the other hand, in the description of the Millennium Prize Problem for the Navier–Stokes equations, Fefferman [11] writes: “Many numerical computations appear to exhibit blow-up for solutions of the Euler equations, but the extreme numerical instability of the equations makes it very hard to draw reliable conclusions.” Indeed, in numerical simulations of hydrodynamics, it is challenging to determine if the behavior you see persists in exact solutions or is a numerical artifact. How does blow-up manifest itself in computer simulations, and how can we distinguish it from computational instability? We need a guideline for how to experimentally, via numerical simulations, recognize blow-up phenomena.

The purpose of this paper is to identify numerical signatures of blow-up. The approach is to carry out numerical experiments for an equation where we expect instant blow-up: the *complexified Euler equations*, suggested by Šverák [22] as the natural complexification of Arnold’s [2] geometric description of Euler’s equations. The equations are

$$(1) \quad \begin{aligned} \frac{\partial v}{\partial t} + \nabla_{\bar{v}} v + \nabla_v^\top \bar{v} &= -\nabla p, \\ \operatorname{div} v &= 0, \end{aligned}$$

[†]Corresponding author.

where v is a time-dependent complexified vector field, p is a complex-valued function, \bar{v} denotes the conjugated vector field, and ∇_v^\top denotes the adjoint of the complexified covariant derivative ∇_v relative to the standard L^2 -pairing.

The interest in the complexified Euler equations (1) arises in their analysis, contrasted against the real setting. Namely, the 2-D (real) Euler equations are globally well-posed, but Šverák noticed that this global analysis does not extend to the complexified 2-D equations. Indeed, Albritton and Ogden [1] showed that the complexified Euler equations (1) on the doubly periodic square are ill-posed with instant blow-up (see details below). We thus have a candidate set of equations for studying how blow-up manifests itself in numerical simulations.

A key question is how to discretize the equations. Just as small modifications of the equations can entirely change the analysis, one discretization to another can gravely affect the convergence behavior relative to blow-up. In particular, for the 2-D complex Euler equations modified to the 2-D complex Navier-Stokes equations by adding a small amount of viscosity, it is expected that the standard well-posedness techniques for Navier-Stokes apply. As Šverák points out, “This is no longer the case for the 2-D complex Euler equation, where the standard proofs of existence depend on more detailed properties of vorticity, which may not be shared by the complex equation.” [22] The result of Albritton and Ogden verifies this statement and indeed makes it precise. Consequently, to identify blow-up in the numerics, we better use a discretization that does not introduce artificial numerical viscosity, which unfortunately the standard discretizations for hyperbolic PDEs do (to achieve stability). We need instead a discretization that captures the hyperbolic nature of the equations, and preferably also the underlying geometric structure identified by Arnold.

Zeitlin’s model [23, 24] is exactly such a method. It is a spatial discretization of the vorticity formulation of the 2-D Euler equations based on quantization theory (*cf.* [5, 6, 13, 15]). Our goals are thus first to extend Zeitlin’s model to the 2-D complex Euler equations (1) and then to identify computationally stable numerical blow-up traits. Zeitlin’s model was originally derived for the flat 2-torus (doubly periodic square), but the technique is conceptually easier and works better for the 2-sphere [21]. Hence, we focus on the complex Euler equations (1) on the 2-sphere, for which we expect the same blow-up properties as on the flat 2-torus.

We now continue the introduction with a brief recollection of the standard Euler equations in 2-D and the basic idea behind Zeitlin’s model.

Via the vorticity function $\omega = \text{curl } v$, the Euler equations on the sphere can be written

$$(2) \quad \frac{\partial \omega}{\partial t} + \{\psi, \omega\} = 0, \quad \Delta \psi = \omega,$$

where $\{\cdot, \cdot\}$ is the Poisson bracket. The velocity field v is recovered from the stream function ψ by the skew gradient $v = \nabla^\top \psi$. Based on the notion of quantization, where functions are replaced by operators (in this case matrices) and the Poisson bracket is replaced by the commutator, Zeitlin’s model for the vorticity equation (2) is the finite-dimensional isospectral matrix flow

$$(3) \quad \frac{dW}{dt} + \frac{1}{\hbar}[P, W] = 0, \quad \Delta_N W = P.$$

Here, the *vorticity matrix* W and the *stream matrix* P are skew-Hermitian $N \times N$ matrices, and $\hbar = 2/\sqrt{N^2 - 1}$. The operator Δ_N is the *Hoppe–Yau Laplacian* [14], corresponding to the Casimir element for a finite-dimensional $\mathfrak{so}(3)$ -representation, just as the Laplace–Beltrami operator on the sphere is the Casimir element for the infinite-dimensional representation of $\mathfrak{so}(3)$ on the space of smooth functions. For more details on Zeitlin’s model (3) and its

geometric properties, see Zeitlin [23, 24], Modin and Viviani [18, 20], and Modin and Perrot [17]. Gallagher [12] established convergence of solutions of Zeitlin’s model to solutions of the vorticity equation for the torus case originally considered by Zeitlin. The convergence in the spherical case was established by Modin and Viviani [21].

The paper is organized as follows. In section 2, we provide some geometric preliminaries needed for the later presentation. The complexified Euler equations together with some properties are given in section 3. The extended Zeitlin discretization for the complexified Euler equations is derived in section 4. Finally, in section 5, we perform numerical experiments, discuss blow-up signatures, and investigate computational stability.

Acknowledgments. This work was supported by the Swedish Research Council (grant number 2022-03453), the Knut and Alice Wallenberg Foundation (grant number WAF2019.0201), and by the Wallenberg AI, Autonomous Systems and Software Program (WASP) funded by the Knut and Alice Wallenberg Foundation. The computations were enabled by resources provided by the National Academic Infrastructure for Supercomputing in Sweden (NAISS), partially funded by the Swedish Research Council through grant agreement no. 2022-06725.

2. GEOMETRIC PRELIMINARIES

In this section, we describe the geometric setting underlying the 2-D Euler equations on the sphere. First, the sphere \mathbb{S}^2 is a Kähler manifold: its area-form is a symplectic form Ω compatible with the standard round metric g via an integrable almost complex structure $J: T\mathbb{S}^2 \rightarrow T\mathbb{S}^2$, i.e., a smooth field of automorphisms of the tangent bundle such that $J^2 = -\text{id}$ and $g(\cdot, \cdot) = -\Omega(J\cdot, \cdot)$.

The gradient ∇f of a smooth function $f \in C^\infty(\mathbb{S}^2, \mathbb{R})$ is defined by

$$df(\cdot) = g(\nabla f, \cdot),$$

where d is the exterior derivative. The Hamiltonian vector field X_f of f is similarly defined by the relation

$$df(\cdot) = \Omega(X_f, \cdot).$$

Since

$$df(\cdot) = g(\nabla f, \cdot) = -\Omega(J\nabla f, \cdot),$$

we have that $-J\nabla f = X_f$. This means that Hamiltonian vector fields are obtained by point-wise $\pi/2$ rotation of corresponding gradient vector fields.

Quantization unfolds from the Poisson algebra of smooth functions $(C^\infty(\mathbb{S}^2, \mathbb{R}), \{\cdot, \cdot\})$, where the Poisson bracket $\{\cdot, \cdot\}: C^\infty(\mathbb{S}^2, \mathbb{R}) \times C^\infty(\mathbb{S}^2, \mathbb{R}) \rightarrow C^\infty(\mathbb{S}^2, \mathbb{R})$ is defined by

$$(4) \quad \{f, g\} = \Omega(X_f, X_g) = X_g(f).$$

In the standard, unit radius embedding $\mathbb{S}^2 \subset \mathbb{R}^3$, it is explicitly given by

$$\{f, g\}(\mathbf{r}) = (\mathbf{r} \times \nabla g(\mathbf{r})) \cdot \nabla f(\mathbf{r}).$$

We sometimes also use spherical coordinates, with the convention

$$(x_1, x_2, x_3) = (\sin \theta \cos \phi, \sin \theta \sin \phi, \cos \theta),$$

where $(\theta, \phi) \in (0, \pi) \times (0, 2\pi)$. In these coordinates, away from the poles, $\nabla f = (\partial_\theta f, \partial_\phi f / \sin \theta)$.

The Poisson bracket is skew-symmetric and satisfies Leibniz's rule and the Jacobi identity. In particular, it is a Lie bracket. Further,

$$(5) \quad [X_f, X_g]_{\mathfrak{X}} = -X_{\{f,g\}},$$

where $[\cdot, \cdot]_{\mathfrak{X}}$ is the Lie bracket of vector fields. Equation (5) means that $f \mapsto X_f$ is a Lie algebra anti-morphism between $(C^\infty(\mathbb{S}^2, \mathbb{R}), \{\cdot, \cdot\})$ and $(\mathfrak{X}_\Omega(\mathbb{S}^2), [\cdot, \cdot]_{\mathfrak{X}})$, where $\mathfrak{X}_\Omega(\mathbb{S}^2)$ denotes Hamiltonian vector fields on \mathbb{S}^2 . The space of all vector fields is denoted $\mathfrak{X}(\mathbb{S}^2)$. Thus, $\mathfrak{X}_\Omega(\mathbb{S}^2)$ is a subalgebra of $\mathfrak{X}(\mathbb{S}^2)$.

3. THE COMPLEXIFIED EULER EQUATIONS

The complexified Euler equations arise naturally as the *Euler–Arnold equations* (cf. [3]) on the complexification of the Lie algebra of Hamiltonian vector fields, as derived by Šverák [22].

In general, if \mathfrak{g} is a real Lie algebra, finite or infinite dimensional, its complexification $\mathfrak{g}_{\mathbb{C}} = \mathfrak{g} \otimes \mathbb{C}$ consists of elements of the form $X + iY$, where $X, Y \in \mathfrak{g}$. The corresponding complexified Lie bracket is thus given by

$$(6) \quad [X_1 + iY_1, X_2 + iY_2]_{\mathbb{C}} = [X_1, X_2] - [Y_1, Y_2] + i[X_1, Y_2] + i[X_2, Y_1].$$

Furthermore, an inner product (\cdot, \cdot) on \mathfrak{g} extends by linearity to a Hermitian inner product on $\mathfrak{g}_{\mathbb{C}}$ whose real part defines an inner product on \mathfrak{g} .

The complexification of $\mathfrak{X}_\Omega(\mathbb{S}^2)$ is $\mathfrak{X}_\Omega(\mathbb{S}^2)_{\mathbb{C}} = \mathfrak{X}_\Omega(\mathbb{S}^2) \otimes \mathbb{C}$. The L^2 -inner product on $\mathfrak{X}_\Omega(\mathbb{S}^2)$ extends to the Hermitian inner product,

$$(7) \quad (v_1, v_2)_{L^2} = \int_{\mathbb{S}^2} v_1 \cdot \overline{v_2},$$

where $v_1, v_2 \in \mathfrak{X}_\Omega(\mathbb{S}^2)_{\mathbb{C}}$. The complexified Euler equations are the Euler–Arnold equations for this inner product. As such, Šverák's [22] derivation is given in terms of the complex vector field v . Next, we give instead a derivation based on complexification of the vorticity formulation (2).

3.1. The complexified vorticity equation. Just as there is a vorticity formulation (2) of the standard 2-D Euler equations, we can derive a vorticity formulation of the 2-D complexified Euler equations (1). It may be obtained by applying curl to equation (1), but more geometrically, we derive it as an Euler–Arnold equation on the complexified symplectic vector fields $\mathfrak{X}_\Omega(\mathbb{S}^2) \otimes \mathbb{C}$. First, the complex vector field v is given as the sum of two real Hamiltonian vector fields, which we see as the Hamiltonian vector field of a complex stream function. Indeed, the Hamiltonian vector field of a purely imaginary function $if \in iC^\infty(\mathbb{S}^2, \mathbb{R})$ is given by

$$X_{if} = iX_f.$$

Thus, given a complex-valued stream function $\psi \in C^\infty(\mathbb{S}^2, \mathbb{C})$, the corresponding complex Hamiltonian vector field is

$$(8) \quad X_\psi = X_{\operatorname{Re} \psi + i \operatorname{Im} \psi} = X_{\operatorname{Re} \psi} + iX_{\operatorname{Im} \psi}.$$

Next, the Poisson algebra structure on $C^\infty(\mathbb{S}^2, \mathbb{C})$ is readily obtained by complexifying $(C^\infty(\mathbb{S}^2, \mathbb{R}), \{\cdot, \cdot\})$. Explicitly, the bracket on $C^\infty(\mathbb{S}^2, \mathbb{C})$ is given by

$$\begin{aligned} \{\psi_1, \psi_2\}_{\mathbb{C}} &= \{\operatorname{Re} \psi_1, \operatorname{Re} \psi_2\} - \{\operatorname{Im} \psi_1, \operatorname{Im} \psi_2\} \\ &\quad + i(\{\operatorname{Im} \psi_1, \operatorname{Re} \psi_2\} + \{\operatorname{Re} \psi_1, \operatorname{Im} \psi_2\}). \end{aligned}$$

By properties inherited from the real-valued case, $(C^\infty(\mathbb{S}^2, \mathbb{C}), \{\cdot, \cdot\}_{\mathbb{C}})$ is a Poisson algebra.

The infinitesimal action of a Hamiltonian vector field on an imaginary function is determined by the Poisson bracket. Indeed, we have that

$$X_{ig}(f) = i\{f, g\},$$

where $f, g \in C^\infty(\mathbb{S}^2, \mathbb{R})$. Thus, for $\psi_1, \psi_2 \in C^\infty(\mathbb{S}^2, \mathbb{C})$,

$$\begin{aligned} (9) \quad X_{\psi_2}(\psi_1) &= X_{\operatorname{Re} \psi_2}(\psi_1) + iX_{\operatorname{Im} \psi_2}(\psi_1) \\ &= X_{\operatorname{Re} \psi_2}(\operatorname{Re} \psi_1) + iX_{\operatorname{Re} \psi_2}(\operatorname{Im} \psi_1) + X_{i\operatorname{Im} \psi_2}(\operatorname{Re} \psi_1) + iX_{i\operatorname{Im} \psi_2}(\operatorname{Im} \psi_1) \\ &\quad + i(\{\operatorname{Re} \psi_1, \operatorname{Im} \psi_2\} + \{\operatorname{Im} \psi_1, \operatorname{Re} \psi_2\}) = \{\psi_1, \psi_2\}_{\mathbb{C}}. \end{aligned}$$

By the definition of the real Lie bracket of vector fields and equation (9), one shows that the Lie bracket of complexified vector fields is related to the complex Poisson bracket by

$$(10) \quad -X_{\{\psi_1, \psi_2\}_{\mathbb{C}}} = [X_{\psi_1}, X_{\psi_2}]_{\mathfrak{X} \otimes \mathbb{C}}.$$

Equation (10) does not define an isomorphism. Indeed, all constant functions are mapped to the zero vector field. Since constant functions form the center of the Poisson algebra $(C^\infty(\mathbb{S}^2, \mathbb{C}), \{\cdot, \cdot\}_{\mathbb{C}})$, we obtain that the reduced Poisson algebra $(C^\infty(\mathbb{S}^2, \mathbb{C})/\mathbb{C}, \{\cdot, \cdot\}_{\mathbb{C}})$ is Lie algebra anti-isomorphic to $\mathfrak{X}_\Omega(\mathbb{S}^2)_{\mathbb{C}}$.

On a general Lie algebra \mathfrak{g} , the Euler–Arnold equations are

$$(11) \quad \frac{d\mu}{dt} = \operatorname{ad}_{dH(\mu)}^* \mu,$$

where $\mu \in \mathfrak{g}^*$ and $H \in C^\infty(\mathfrak{g}^*, \mathbb{R})$ is the Hamiltonian function with exterior derivative $dH(\mu) \in \mathfrak{g}^{**} \simeq \mathfrak{g}$. The mapping $\operatorname{ad}^*: \mathfrak{g} \rightarrow \operatorname{End}(\mathfrak{g}^*)$ is the dual, under the canonical dual pairing, of the adjoint representation $\operatorname{ad}: \mathfrak{g} \rightarrow \operatorname{End}(\mathfrak{g})$. This way, equation (1) is retrieved with $\mathfrak{g} = \mathfrak{X}_\Omega(\mathbb{S}^2)_{\mathbb{C}}$ and the Hamiltonian

$$(12) \quad H(v) = \frac{1}{2}(v, v)_{L^2}.$$

As mentioned, the mapping $\psi \mapsto X_\psi$ provides an isomorphism between the two Lie algebras $(C^\infty(\mathbb{S}^2, \mathbb{C})/\mathbb{C}, \{\cdot, \cdot\}_{\mathbb{C}})$ and $\mathfrak{X}_\Omega(\mathbb{S}^2)_{\mathbb{C}}$, which yields the following.

Proposition 3.1. *The vorticity formulation of equation (1) is,*

$$(13) \quad \frac{\partial \omega}{\partial t} = \{-\bar{\psi}, \omega\}_{\mathbb{C}}, \quad -\Delta \psi = \omega.$$

Proof. The first step towards a complexified vorticity formulation of equation (1) is to derive the corresponding Euler–Arnold equation on $(C^\infty(\mathbb{S}^2, \mathbb{C})/\mathbb{C}, \{\cdot, \cdot\}_{\mathbb{C}})$. As the Euler–Arnold equation evolves on the dual of the algebra, we note that the (smooth) dual of $(C^\infty(\mathbb{S}^2, \mathbb{C})/\mathbb{C}, \{\cdot, \cdot\}_{\mathbb{C}})$ is the annihilator of constant functions in the space of top-forms. A top-form $\beta = \omega \Omega$, where $\omega \in C^\infty(\mathbb{S}^2, \mathbb{C})$, acts on a function $\psi \in C^\infty(\mathbb{S}^2, \mathbb{C})$ by

$$(14) \quad \langle \beta, \psi \rangle = \int_{\mathbb{S}^2} \omega \bar{\psi}.$$

Since top-forms can be identified with smooth functions, the (smooth) dual of $C^\infty(\mathbb{S}^2, \mathbb{C})/\mathbb{C}$ is isomorphic to $C_0^\infty(\mathbb{S}^2, \mathbb{C})$, the smooth complex-valued functions with vanishing mean.

The next step is to compute $\text{ad}_\psi^* : C_0^\infty(\mathbb{S}^2, \mathbb{C}) \rightarrow C_0^\infty(\mathbb{S}^2, \mathbb{C})$. By definition,

$$\begin{aligned} \langle \text{ad}_\psi^* \omega, \xi \rangle &= \langle \omega, \text{ad}_\psi \xi \rangle = \int_{\mathbb{S}^2} \omega \overline{\{\psi, \xi\}_{\mathbb{C}}} = \int_{\mathbb{S}^2} \omega \{\bar{\psi}, \bar{\xi}\}_{\mathbb{C}} = \\ &= \int_{\mathbb{S}^2} (\{\bar{\psi}, \omega \bar{\xi}\}_{\mathbb{C}} - \bar{\xi} \{\bar{\psi}, \omega\}_{\mathbb{C}}) = \langle \{-\bar{\psi}, \omega\}_{\mathbb{C}}, \xi \rangle, \end{aligned}$$

where, in the fourth equality, Leibniz's rule is used. Therefore,

$$(15) \quad \text{ad}_\psi^* \omega = \{-\bar{\psi}, \omega\}_{\mathbb{C}}$$

The final step is to find the canonical relationship between ω and ψ determined by the Hamiltonian of the complexified Euler equation, i.e., equation (12).

The Hamiltonian $\tilde{H} : C_0^\infty(\mathbb{S}^2, \mathbb{C}) \rightarrow \mathbb{R}$ is given by

$$(16) \quad \tilde{H}(\omega) = \frac{1}{2} \int_{\mathbb{S}^2} X_\psi \cdot \bar{X}_\psi.$$

Since

$$\int_{\mathbb{S}^2} X_\psi \cdot \bar{X}_\psi = \int_{\mathbb{S}^2} \nabla \psi \cdot \nabla \bar{\psi},$$

integration by parts yields that equation (16) becomes

$$(17) \quad \tilde{H}(\omega) = \frac{1}{2} \int_{\mathbb{S}^2} -\Delta \psi \bar{\psi},$$

so $\tilde{H}(\omega) = \frac{1}{2}(-\Delta \psi, \psi)_{L^2}$, and we have that

$$(18) \quad d\tilde{H}(\omega) = -\Delta^{-1} \omega,$$

Therefore, by inserting equations (15) and (18) into the abstract formulation (11), we see that the vorticity equation is given by equation (13). \square

3.2. Properties of the complexified Euler equations. We first remark that there are several conserved quantities. First, note that the Hamiltonian (12) (i.e., the kinetic energy) is conserved. Furthermore, the complex vorticity formulation (13) reveals an infinite set of Casimir functions: if $f : \mathbb{C} \rightarrow \mathbb{C}$ is a holomorphic function, then

$$(19) \quad C_f(\omega) = \int_{\mathbb{S}^2} f(\omega)$$

is conserved. Indeed,

$$\frac{d}{dt} C_f(\omega) = \int_{\mathbb{S}^2} f'(\omega) \{-\bar{\psi}, \omega\}_{\mathbb{C}} = \int_{\mathbb{S}^2} \bar{\psi} \{f'(\omega), \omega\}_{\mathbb{C}},$$

which vanishes since f' can be expanded in a Taylor series and $\{\omega^k, \omega\}_{\mathbb{C}} = 0$. The Casimirs (19) reveal a special structure of the complexified Euler equations in two dimensions, analogous to the special structure of the real Euler equations in two dimensions.

Moreover, we note that if the initial value is real, then the vorticity remains real and the complexified vorticity equations (13) reduce to the standard vorticity equations (2). Indeed, equation (13) separates neatly into components: with $\omega = \omega_R + i\omega_I$ and $\psi = \psi_R + i\psi_I$ it can be written

$$\begin{aligned} \dot{\omega}_R &= -\{\psi_R, \omega_R\} - \{\psi_I, \omega_I\} \\ \dot{\omega}_I &= -\{\psi_R, \omega_I\} + \{\psi_I, \omega_R\}. \end{aligned}$$

4. ZEITLIN'S MODEL FOR THE COMPLEXIFIED EULER EQUATIONS

In this section, we show how a finite-dimensional analogue of the developments in the previous section naturally leads to a generalization of Zeitlin's approach to the vorticity formulation (13) of the complexified Euler equation on \mathbb{S}^2 .

We first review how the Poisson algebra $(C^\infty(\mathbb{S}^2, \mathbb{C}), \{\cdot, \cdot\})$ is discretized via quantization. Further details are found in the papers by Hoppe and Yau [14] and by Modin and Viviani [18, 21].

The vorticity equation evolves on the (smooth) dual of the space of symplectic vector fields. The quantized equation should have an equivalent structure: it should evolve on the dual of a matrix Lie algebra. To obtain the quantization scheme, we use a matrix analog of the Laplacian, as given by Hoppe and Yau [14]. It is an operator $\Delta_N: \mathfrak{sl}(N, \mathbb{C}) \rightarrow \mathfrak{sl}(N, \mathbb{C})$ which allows us to build an eigenbasis of $\mathfrak{sl}(N, \mathbb{C})$ corresponding to the spherical harmonic basis of functions on \mathbb{S}^2 .

Explicitly, we begin with a spin $\frac{N-1}{2}$ representation of $\mathfrak{so}(3)$ in $\mathfrak{u}(N)$. Its generators X_1, X_2, X_3 satisfy the commutation relations of $\mathfrak{so}(3)$ up to scaling by $\hbar_N = 2/\sqrt{N^2 - 1}$:

$$\begin{aligned} [X_1, X_2] &= \hbar_N X_3, \\ [X_3, X_1] &= \hbar_N X_2, \\ [X_2, X_3] &= \hbar_N X_1. \end{aligned}$$

The infinite-dimensional analogue is the following. Via the natural embedding $\mathbb{S}^2 \subset \mathbb{R}^3$, there is a representation of $\mathfrak{so}(3)$ in $C^\infty(\mathbb{S}^2, \mathbb{R})$, with generators given by the coordinate functions x_1, x_2, x_3 . They each generate rotations about their respective coordinate axis. This representation satisfies the commutation relations of $\mathfrak{so}(3)$,

$$\begin{aligned} \{x_1, x_2\} &= x_3, \\ \{x_3, x_1\} &= x_2, \\ \{x_2, x_3\} &= x_1. \end{aligned}$$

Moreover, the Laplace–Beltrami operator on \mathbb{S}^2 can be expressed in terms of the Poisson bracket and the generators as

$$(20) \quad \Delta = \sum_{k=1}^3 \{x_k, \{x_k, \cdot\}\}.$$

Analogous to this expression for Δ , the Hoppe–Yau Laplacian on $\mathfrak{sl}(N, \mathbb{C})$ is defined by

$$(21) \quad \Delta_N = \frac{1}{\hbar_N^2} \sum_{k=1}^3 [X_k, [X_k, \cdot]].$$

The eigenvalues of the Hoppe–Yau Laplacian Δ_N coincide with the first N^2 eigenvalues of the Laplace–Beltrami operator Δ , see [14]. The quantization of a function $\zeta \in C^\infty(\mathbb{S}^2, \mathbb{C})$ is now given by a mapping from $C^\infty(\mathbb{S}^2, \mathbb{C})$ to $\mathfrak{gl}(N, \mathbb{C})$ as follows.

The expansion of ζ in the spherical harmonics $\{Y_{l,m} \mid l \geq 0, m = -l, \dots, l\}$ is truncated,

$$\zeta^N = \sum_{l=0}^N \sum_{m=-l}^l c_{l,m} Y_{l,m}.$$

The quantization is then performed by identifying the first N^2 spherical harmonics, being eigenfunctions of Δ , with corresponding eigen-matrices of Δ_N , denoted $T_{l,m}^N$. Once such a correspondence is established, we obtain a mapping from functions to matrices via

$$\zeta^N \mapsto Z = \sum_{l=0}^N \sum_{m=-l}^l c_{l,m} T_{l,m}^N.$$

It remains to describe the matrices $T_{l,m}^N$. The quantized Laplacian Δ_N maps $\pm m$ -diagonal matrices to $\pm m$ -diagonal matrices. A unique eigenbasis to Δ_N is given if we take $T_{l,m}$ to be $\pm m$ -diagonal. Under this restriction, the eigenvalue problem

$$\Delta_N T_{l,m}^N = -l(l+1) T_{l,m}^N$$

has a unique solution up to sign. We determine the sign based on the corresponding continuous harmonics $Y_{l,m}$. This process provides a quantization of complex-valued functions. From the point of view of complexification, just as $C^\infty(\mathbb{S}^2, \mathbb{C}) \simeq C^\infty(\mathbb{S}^2, \mathbb{R}) \otimes \mathbb{C}$, the quantized equivalent of complex-valued functions is $\mathfrak{gl}(N, \mathbb{C}) \simeq \mathfrak{u}(N) \otimes \mathbb{C}$.

In direct analogue to the previous section, we also obtain the ad_P^* operator on $\mathfrak{sl}(N, \mathbb{C})$ via

$$\langle \text{ad}_P^* W, X \rangle = \text{tr}(W[P, X]^*) = \text{tr}(-W[P^*, X^*]) = \text{tr}([P^*, W]X^*) = \langle [P^*, W], X \rangle.$$

Thus, for $P \in \mathfrak{sl}(N, \mathbb{C})$ and $W \in \mathfrak{sl}(N, \mathbb{C})$, $\text{ad}_P^* W = [P^*, W]$, which is well-defined on $\mathfrak{sl}(N, \mathbb{C})$, since \mathbb{C}^*I is the center of $\mathfrak{gl}(N, \mathbb{C})$. Notice that classical conjugation $\psi \mapsto \bar{\psi}$ corresponds in the quantized framework to $P \mapsto -P^*$.

4.1. Matrix vorticity equations. We are now in position to state the spatially discretized version of the vorticity formulation (13) of the complexified Euler equations on \mathbb{S}^2 . Indeed, the equations are

$$(22) \quad \frac{dW}{dt} = \frac{1}{\hbar_N} [P^*, W], \quad -\Delta_N P = W,$$

where $-\Delta_N$ is a bijective operator $\mathfrak{sl}(N, \mathbb{C}) \rightarrow \mathfrak{sl}(N, \mathbb{C})$.

Notice that an initially skew-Hermitian solution remains skew-Hermitian. Indeed, equation (22) separate into skew-Hermitian and Hermitian components, just as the complexified vorticity equation (13) separates into real and imaginary components.

We remark that the matrix vorticity equations (22) are still not fully discrete: a time discretization is needed, i.e., a numerical integrator. To ensure that the geometric structure of Euler-Arnold equations are properly reflected in the numerics, it is advisable to use an integrator that preserves the Lie–Poisson structure. See, for instance, Engø and Faltinsen [10], Bogfjellmo and Marthinsen [4], and Modin and Viviani [19] for examples of such integrators.

Remark 4.1. *The matrix vorticity equations (22) preserve the structure that leads to the Casimirs (19). Indeed, if f is holomorphic, then*

$$(23) \quad C_f^N(W) = \text{tr}(f(W))$$

is a Casimir. These Casimirs reflect that the flow is isospectral.

5. NUMERICAL STUDY OF BLOW-UP

We now numerically study the blow-up of the complexified Euler equations on \mathbb{S}^2 . To this end, we first remark that any purely real solution (in the Zeitlin case, purely skew-Hermitian) to the complexified Euler equations devolves to the real Euler equations. Therefore, we focus on perturbations of purely imaginary stationary solutions (in the matrix case, purely Hermitian). Indeed, the blow-up of the complexified Euler equations arises from instability of the interaction of the real and imaginary components.

In the numerical study, we use the matrix vorticity equations (22). We consider initial conditions of the form $W_0 = \hat{W}_0 + \mathcal{E}_0$, where \hat{W}_0 results in a stationary flow and \mathcal{E}_0 is a small random perturbation. Zonal flows are a natural choice for the initial condition, as zonal flows are stationary solutions to the Euler equations. To this end, we select a second imaginary quantized zonal flow as a starting point to build the initial condition, i.e., we let the Hermitian part of \hat{W}_0 be $T_{2,0}$ and set the skew-Hermitian part to zero. Further,

$$\mathcal{E}_0 = \varepsilon \sum_{l=0}^N \sum_{m=-l}^l c_{l,m} T_{l,m}^N,$$

Here, ε is a small real number, in all simulations chosen to be 0.1, and $c_{l,m}$ are random complex numbers chosen such that the real and imaginary parts are independent normal random variables with mean 0 and variance such that

$$\text{Var} \sum_{l=0}^N \sum_{m=-l}^l \text{Re } c_{l,m} = \text{Var} \sum_{l=0}^N \sum_{m=-l}^l \text{Im } c_{l,m} = 1,$$

so that the variance of the perturbation is independent of N . All in all, we end up with a random noisy initial condition as the skew-Hermitian part, shown in figure 1a and a perturbed zonal initial condition in the Hermitian part, depicted in figure 2a.

We apply the isospectral midpoint method of [18] to equation (22) to numerically integrate the equations in time. The method is a Lie–Poisson integrator that preserves the Lie–Poisson structure of the equations, and in particular, the Casimirs. Each step of the integration is given by

$$(24) \quad \begin{aligned} W_n &= \left(I - \frac{\delta t}{2\hbar_N} \Delta_N^{-1} \widetilde{W} \right) \widetilde{W} \left(I + \frac{\delta t}{2\hbar_N} \Delta_N^{-1} \widetilde{W} \right), \\ W_{n+1} &= \left(I - \frac{\delta t}{2\hbar_N} \Delta_N^{-1} \widetilde{W} \right) \widetilde{W} \left(I + \frac{\delta t}{2\hbar_N} \Delta_N^{-1} \widetilde{W} \right), \end{aligned}$$

where I is the identity matrix and \widetilde{W} is an intermediate variable obtained by solving the first implicit step. In the simulations, we compute \widetilde{W} at each step by fixed-point iterations with a time step size of $\delta t = 10^{-5} \hbar_N$.

For $N = 256$, figures 1 and 2 show snapshots of the evolution of W until “numerical blow-up”, which we take to be when the spectral norm¹ of W exceeds 10^{13} . This threshold for blow-up is reached at $t = 0.04619$, after 591 232 integration steps. As the solution becomes increasingly larger, we observe that the maximum vorticity clusters in bands corresponding to the areas where the Hermitian part of the initial conditions are vanishing. This observation

¹The spectral norm of the matrices corresponds to the L^∞ -norm of the corresponding vorticity functions.

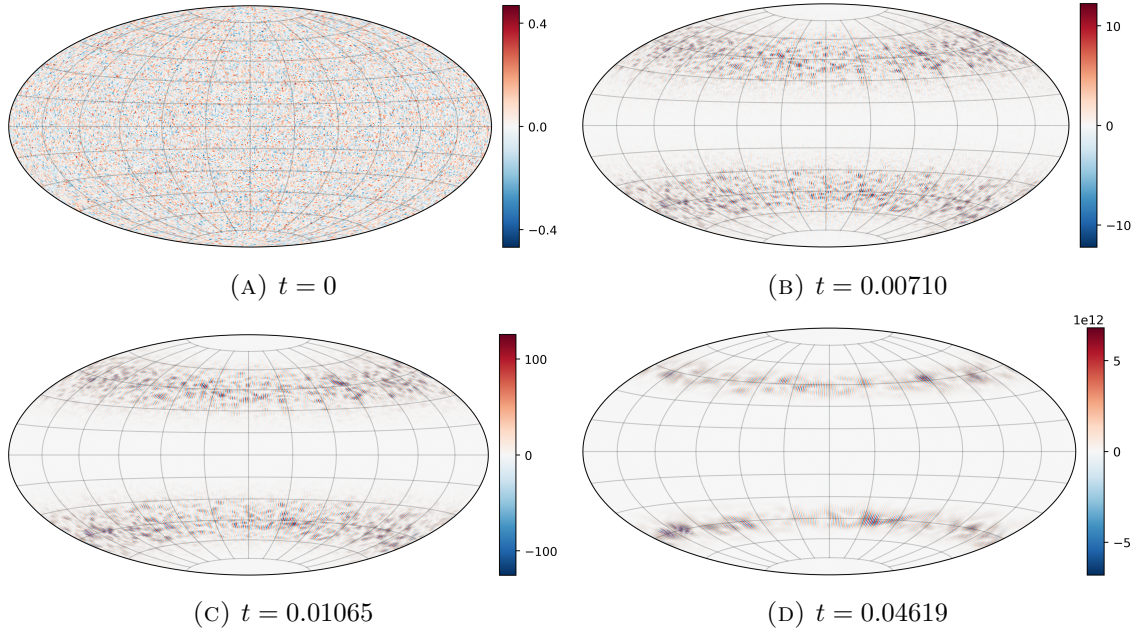


FIGURE 1. The skew-Hermitian part (real component) of the vorticity matrix. Note that, while the component is initially small, it grows rapidly and reaches numerical blow-up at $t = 0.04619$.

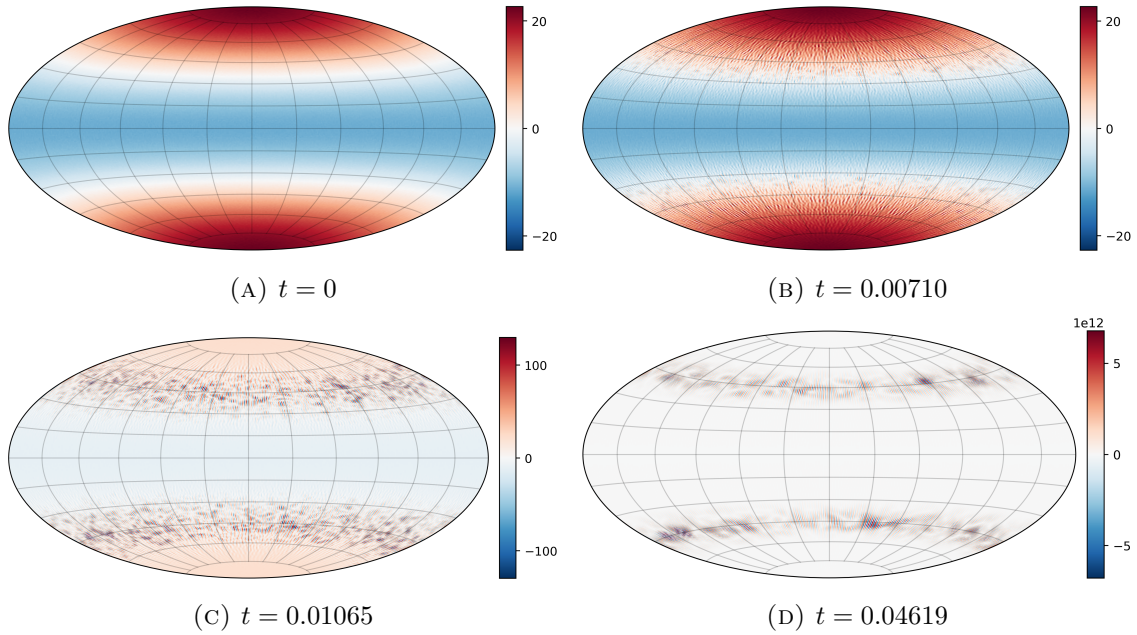


FIGURE 2. The Hermitian part (imaginary component) of the vorticity matrix. It grows rapidly and reaches numerical blow-up at $t = 0.04619$.

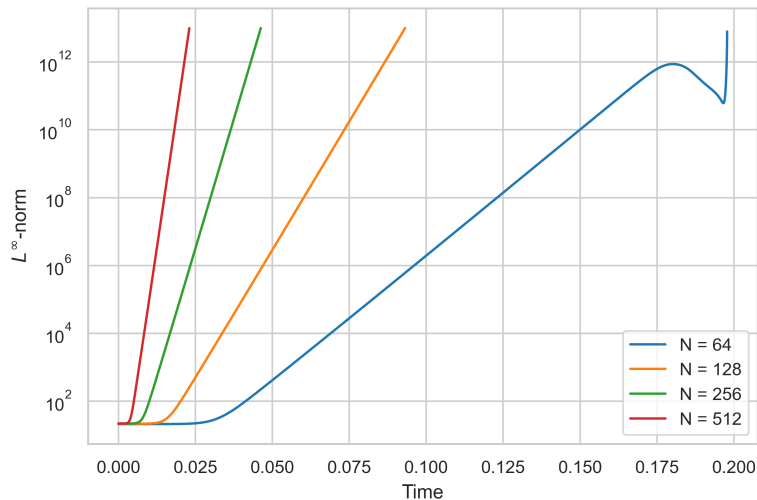


FIGURE 3. The growth in time of the spectral norm for the $N = 256$ solution displayed in figures 1 and 2, together with the corresponding growths for solutions with $N = 64, 128, 512$.

conforms with the proposed blow-up mechanisms of 3-D Euler, which happen in regions near vanishing vorticity (cf. Drivas and Elgindi [8, sec. 4-5]).

Figure 3 shows the evolution of the spectral norm for the simulation depicted in figures 1 and 2, together with the corresponding growth for simulations with $N = 64, 128, 256, 512$. We observe exponential growth of the norm, with rates increasing with N .

5.1. Experiment 1: The observed blow-up is computationally stable. A question to be resolved is if the observed numerical blow-up is the result of discretization artifacts, such as rounding errors or computational instability, or if the observations in figures 1 to 3 truly are indicative of blow-up. We present here three arguments and further simulations strongly suggesting the latter.

First, the conservation of Casimirs is useful as a first check to ensure computational stability regarding round-off errors. Indeed, nowhere in the discretization do we force conservation of Casimirs; they are invariant of the fully discretized dynamical system, which is isospectral. But the realization of this dynamical system in the computer is not over the field \mathbb{C} of complex numbers, but over an approximation by floating-point numbers prone to round-off errors. Furthermore, the time-discretization scheme (24) is implicit, so it needs an iterative solver (e.g., Newton’s method of fixed-point iterations) and these iterations must be truncated. Thus, we cannot expect the Casimirs (23) to be exactly conserved. But they should be preserved up to floating-point round-off errors (i.e., the machine precision). Equivalently, since the Casimir preservation is a consequence of isospectrality of the matrix vorticity equations (22), we can check that the eigenvalues are conserved, up to round-off errors. Therefore, as a soundness check of the experimental results, we compute, for each time-step n , the ordered set of eigenvalues of W_n , denoted by $\sigma(W_n) = \{\lambda_1^{W_n}, \lambda_2^{W_n}, \dots, \lambda_N^{W_n}\}$. Thereafter, we

record the maximum absolute deviation of $\sigma(W_n)$ from $\sigma(W_0)$, i.e.,

$$d_n = \max_{i=1,\dots,N} |\lambda_i^{W_n} - \lambda_i^{W_0}|.$$

If d_n is preserved up to machine precision for all n , it gives us a strong indication that there are no numerical artifacts due to floating-point overflow (i.e., significant inaccuracies in the floating-point approximations). To compensate for any spurious effects of the random initial condition, we repeat the experiment 10 times. The result is that d_n is preserved up to machine precision in all computed time steps (these results are unenlightening to visualize).

Secondly, we notice that the matrix vorticity equations (22) constitute a reversible system. Furthermore, this reversibility is preserved by the Lie-Poisson time-discretization (24). Therefore, by reversing the arrow of time, by changing the sign of the time step, we should be able to stop the simulation at any point and run the simulation backwards to recover the initial condition. If the blow-up is due to an accumulation of round-off errors, we should not be able to achieve this, since the floating-point operations certainly are not exactly reversible.

We thus perform a second simulation, using as initial data the final vorticity of the simulation depicted in figures 1d and 2d. The time step is now negative $\delta t = -10^{-5}\hbar_N$, thereby reversing the arrow and time, and we run the simulations again for 591 232 time steps, corresponding to back-tracking to $t = 0$. The results are given in figures 4 and 5. We observe that the initial vorticity configuration is recovered, in the sense that it is visually indistinguishable from the first initial data. The simulations are therefore computationally reversible. As a more quantitative verification, we consider again the evolution of the spectral norm. In figure 6, we see that this time, the spectral norm decreases, at least exponentially, and the inverse pattern to figure 3 holds. We conclude that by the reversing the arrow of time, we can return to the point where we started. Thus, the observed vorticity growth is not due to accumulation of round-off errors.

So far, we have concluded computational stability with respect to round-off errors. Another source of error is, of course, that we discretize in time. Indeed, one could imagine that the numerical blow-up we see is due to instability induced by the time discretization. As a third argument of computational stability, we therefore investigate if the observed vorticity growth is due to a too large a time step size. To this end, we fix $N = 128$ and use four different step sizes, $10^{-3}\hbar_N$, $10^{-4}\hbar_N$, $10^{-5}\hbar_N$ and $10^{-6}\hbar_N$. Again, we run the simulation as above until our threshold for blow-up is reached. We repeat the experiment over 5 runs and plot the mean time to blow-up, together with the 95% quantiles, in figure 7. We remark that the average time to blow-up seems to increase as for the first decrease in step size, where after the increase evens out and seems to settle at around 0.0935. Thus, we conclude that the numerically observed blow-up does not seem to be an artifact of the step size, as it is stable under changes of the step size does not influence the time noticeably for small enough step sizes.

5.2. Experiment 2: Time to blow-up decreases as spatial resolution increases. The numerical simulations in this study do not, of course, display proper blow-up: the spectral norm is finite and, although fast, its growth-rate in time also remains finite. Nor can we expect the matrix vorticity equations (22) to have blow-up. In fact, it is easy to prove that solutions must exist globally in time: in finite dimension all norms are equivalent, and since the Hamiltonian corresponding to the equations (22) is conserved and also constitutes a norm, the spectral norm must be bounded. Indeed, for Euler-Arnold equations, finite time blow-up is necessarily an infinite-dimensional phenomenon. We claim, nevertheless, that our

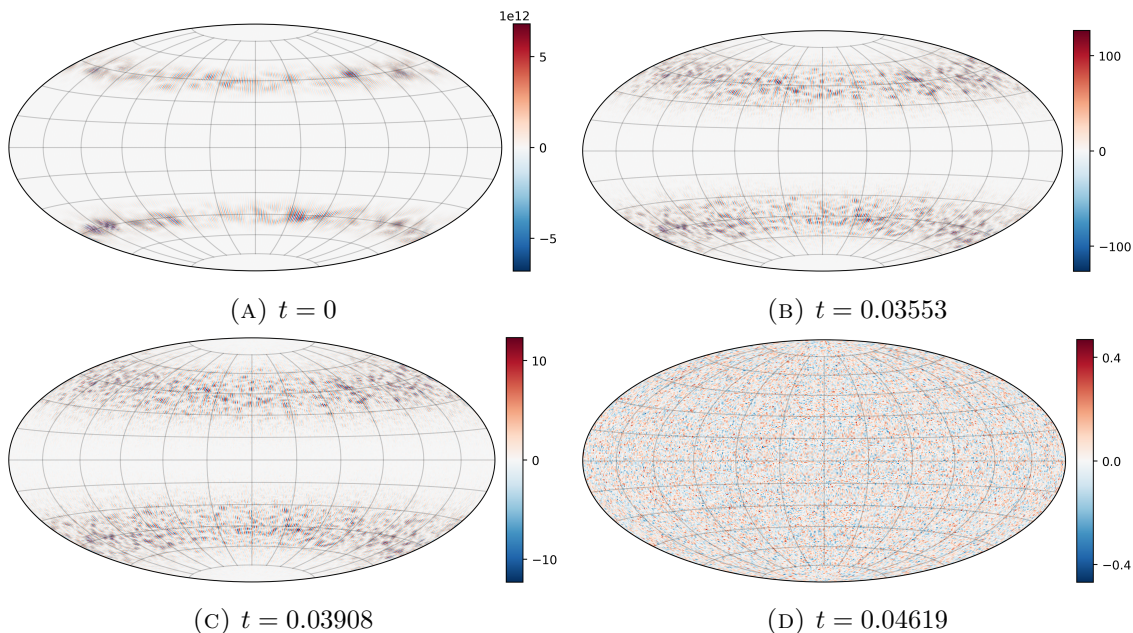


FIGURE 4. The skew-Hermitian part (real component) of the vorticity matrix in the reversed simulation. Note that, while the component is initially at the threshold of blow-up at $T = 0$, it rapidly decreases and has returned to the initial conditions of the first simulation at $T = 0.04619$.

numerical experiments provide strong evidence of genuine blow-up of solutions to the infinite-dimensional system (13).

The key is to carefully study the behavior as the spatial resolution N of the matrix system increases. To this end, we vary N linearly between $N = 32$ and $N = 512$ with increments of 4. We repeat the above procedure, for each N a total of $M = 15$ times, to quantify the uncertainty in the blow-up time induced by the random initial conditions. The time step is set to $\delta t = 10^{-5} \hbar_N$.

The results are shown in figure 8, where the blow-up time is plotted against N . We observe that the blow-up time decreases with N , indicating that the complexified Euler equations are ill-posed, in the sense that the blow-up time tends to zero as the resolution increases. We observe that after a transient phase for low spatial resolutions, the decrease appears to be linear in log-log scale. The regularity of this graph is a further indication of computational stability.

To strengthen the argument, we can return to figure 3. We note that in all cases, after a transient phase in the beginning, the spectral norms grow exponentially (linear in log-scale), but the growth rate depends on N : larger N yields faster norm growth. We remark that for the lower resolution, $N = 64$, the growth halts after a certain time. This is because we work in finite-dimensional spaces, where all norms are equivalent. Therefore, eventually, the value of the norm stabilizes for any N . However, if the dimension of the space is high enough, this happens after we have reached our numerical threshold for blow-up.

Excluding the initial phase as well as the final phase in the case $N = 64$, we estimate the growth rate of the logarithm of the norm and plot these against N in figure 9. We

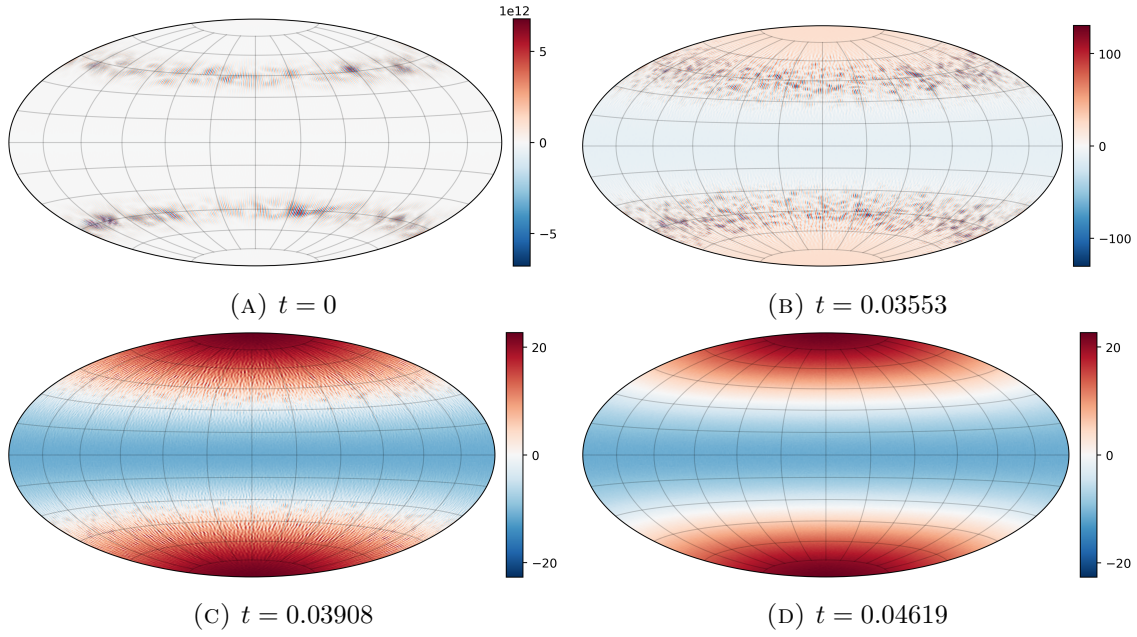


FIGURE 5. The Hermitian part (imaginary component) of the vorticity matrix. Note that, while the component is initially at the threshold of blow-up at $T = 0$, it decreases rapidly and has at $T = 0.04619$ returned to the initial conditions of the first simulation.

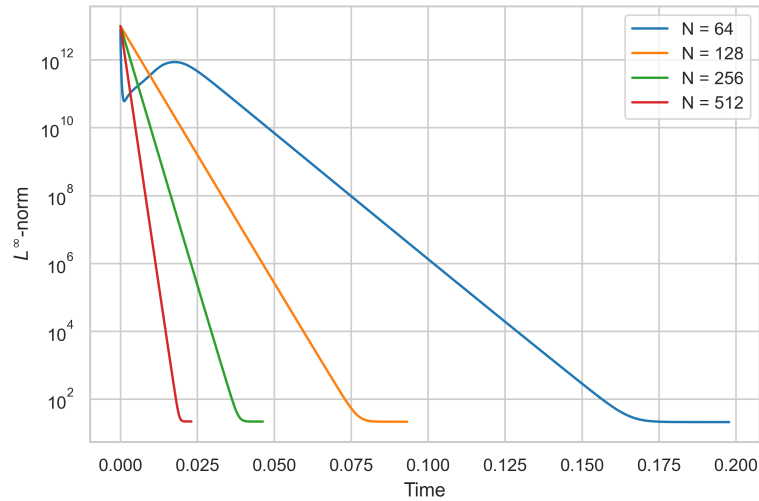


FIGURE 6. The decrease of the L^∞ -norm of the solutions plotted in figures 4 and 5, together with the corresponding decrease for solutions with $N = 64, 128$ and 512.

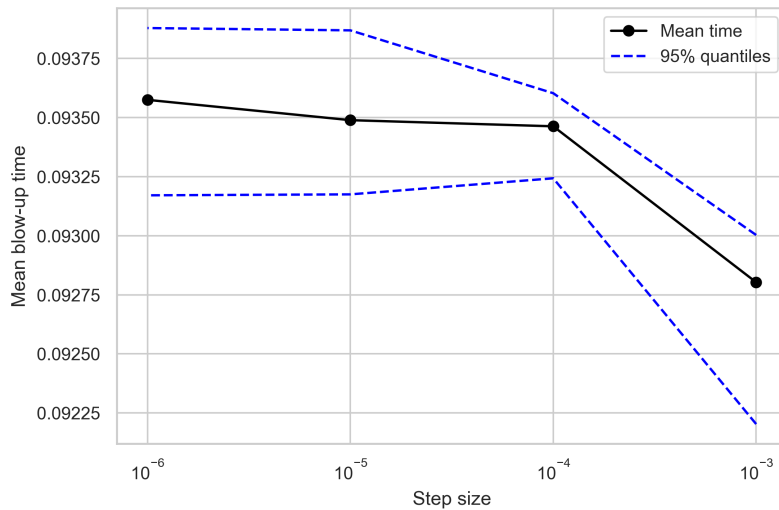


FIGURE 7. The mean time to blow-up over $M = 5$ runs for a range of step sizes. Note that the average time to blow-up is relatively constant for small enough time step sizes.

observe a striking linear relationship between the matrix size and the norm growth rate. This relationship suggests the following recipe as a numerical signature of blow-up:

- (1) First, ensure that the observed behavior is computationally stable by repeating what is described in “Experiment 1” above.
- (2) Second, check the growth-rates in time of the relevant norm for a series of simulations with increasing resolution. If the corresponding graph, such as in figure 9, displays regular, non-deflecting increase of the growth-rates for increasing N , there is convincing numerical evidence of finite time blow-up.

REFERENCES

- [1] ALBRITTON, D., AND OGDEN, W. J. Remarks on the complex Euler equations. *Commun. Pure Appl. Anal.* 0, 0 (2023), 0–0.
- [2] ARNOLD, V. I. Sur la géométrie différentielle des groupes de Lie de dimension infinie et ses applications à l’hydrodynamique des fluides parfaits. *Ann. de l’Institut Fourier* 16, 1 (1966), 319–361.
- [3] ARNOLD, V. I., AND KHESIN, B. A. *Topological Methods in Hydrodynamics*, second ed. Springer Nature, 2021.
- [4] BOGFJELLMO, G., AND MARTHINSEN, H. High-order symplectic partitioned Lie group methods. *Found. Comp. Math.* 16, 2 (May 2015), 493–530.
- [5] BORDEMANN, M., HOPPE, J., SCHALLER, P., AND SCHLICHENMAIER, M. $\mathfrak{gl}(\infty)$ and geometric quantization. *Commun. Math. Phys.* 138, 2 (May 1991), 209–244.
- [6] BORDEMANN, M., MEINRENKEN, E., AND SCHLICHENMAIER, M. Toeplitz quantization of Kähler manifolds and $\mathfrak{gl}(N)$, $N \rightarrow \infty$ limits. *Commun. Math. Phys.* 165, 2 (Oct. 1994), 281–296.
- [7] CHEN, J., AND HOU, T. Y. Finite time blowup of 2D Boussinesq and 3D Euler equations with $C^{1,\alpha}$ velocity and boundary. *Comm. Math. Phys.* 383, 3 (2021), 1559–1667.
- [8] DRIVAS, T. D., AND ELGINDI, T. M. Singularity formation in the incompressible Euler equation in finite and infinite time. *EMS Surv. Math. Sci.* 10, 1 (2023), 1–100.

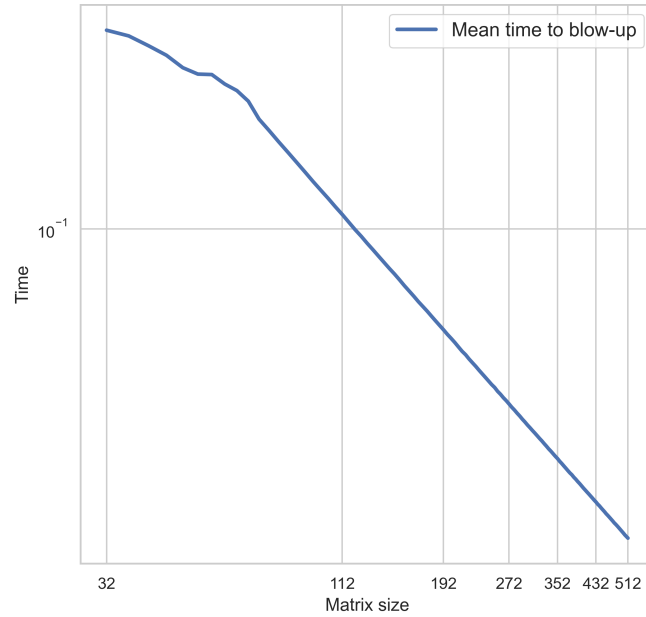


FIGURE 8. The mean time to blow-up over $M = 15$ runs, plotted against the matrix size, plotted on a log-log scale. We define blow-up as the time when the spectral norm exceeds 10^{13} . Note that the blow-up time decays linearly towards zero.

- [9] ELGINDI, T. M. Finite-time singularity formation for $C^{1,\alpha}$ solutions to the incompressible Euler equations on \mathbb{R}^3 . *Ann. Math.* *194*, 3 (2021), 647 – 727.
- [10] ENGØ, K., AND FALTINSEN, S. Numerical integration of Lie–Poisson systems while preserving coadjoint orbits and energy. *SIAM J. Numer. Anal.* *39*, 1 (Jan. 2001), 128–145.
- [11] FEFFERMAN, C. L. Existence and smoothness of the Navier–Stokes equation. <https://www.claymath.org/wp-content/uploads/2022/06/navierstokes.pdf>, June 2022.
- [12] GALLAGHER, I. Mathematical analysis of a structure-preserving approximation of the bidimensional vorticity equation. *Num. Math.* *91*, 2 (2002), 223–236.
- [13] HOPPE, J. Diffeomorphism groups, quantization, and $SU(\infty)$. *Int. J. Mod. Phys. A* *04*, 19 (Nov. 1989), 5235–5248.
- [14] HOPPE, J., AND YAU, S.-T. Some properties of matrix harmonics on \mathbb{S}^2 . *Commun. Math. Phys.* *195*, 1 (July 1998), 67–77.
- [15] LE FLOCH, Y. *A Brief Introduction to Berezin–Toeplitz Operators on Compact Kähler Manifolds*. Springer International Publishing, 2018.
- [16] LUO, G., AND HOU, T. Y. Toward the finite-time blowup of the 3D axisymmetric Euler equations: A numerical investigation. *Multiscale Model. Simul.* *12*, 4 (Jan. 2014), 1722–1776.
- [17] MODIN, K., AND PERROT, M. Eulerian and Lagrangian stability in Zeitlin’s model of hydrodynamics. arxiv:2305.08479, 2023.
- [18] MODIN, K., AND VIVIANI, M. A Casimir preserving scheme for long-time simulation of spherical ideal hydrodynamics. *J. Fluid Mech.* *884* (Dec. 2019).
- [19] MODIN, K., AND VIVIANI, M. Lie–Poisson methods for isospectral flows. *Found. Comp. Math.* *20*, 4 (Aug. 2019), 889–921.

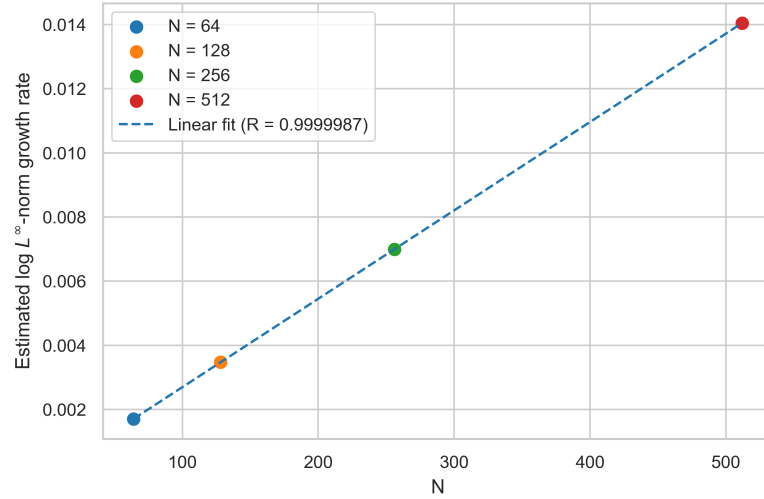


FIGURE 9. The estimated growth rates of the norms. We observe a striking linear relationship between the matrix size N (i.e., the spatial resolution) and the growth rate.

- [20] MODIN, K., AND VIVIANI, M. Canonical scale separation in 2D incompressible hydrodynamics. *J. Fluid Mech.* *943* (2022), A36.
- [21] MODIN, K., AND VIVIANI, M. Two-dimensional fluids via matrix hydrodynamics. arXiv:2405.14282, 2024.
- [22] SVERAK, V. On certain models in the PDE theory of fluid flows. *Journ. Équ. dériv. partielles* (Feb. 2018), 1–26.
- [23] ZEITLIN, V. Finite-mode analogs of 2D ideal hydrodynamics: Coadjoint orbits and local canonical structure. *Physica D* *49*, 3 (Apr. 1991).
- [24] ZEITLIN, V. Self-consistent finite-mode approximations for the hydrodynamics of an incompressible fluid on nonrotating and rotating spheres. *Phys. Rev. Lett.* *93*, 26 (Dec. 2004).

Email address: erikjans@chalmers.se

Email address: klas.modin@chalmers.se

*DEPARTMENT OF MATHEMATICAL SCIENCES, CHALMERS UNIVERSITY OF TECHNOLOGY & UNIVERSITY OF GÖTHEBURG, S-412 96 GÖTEBURG, SWEDEN.